Polymer Chemistry

Accepted Manuscript

ROYAL SOCIETY OF CHEMISTRY

www.rsc.org/polymers

Cite this: DOI: 10.1039/c0xx00000x

www.rsc.org/xxxxxx

ARTICLE TYPE

Precise Modular Synthesis and Structure-Property Study of Acid-Cleavable Star-Block Copolymers for pH-Triggered Drug Delivery

Jian Hu, Jinlin He*, Mingzu Zhang, Peihong Ni*

Received (in XXX, XXX) Xth XXXXXXXXX 20XX, Accepted Xth XXXXXXXXX 20XX

DOI: 10.1039/b000000x

A series of well-defined three-arm star-block copolymers containing poly(ethylene glycol) monomethyl ether (mPEG) and poly(ε-caprolactone) (PCL) blocks linked with acid-cleavable acetal groups, designated as (mPEG-*acetal*-PCL-*acetal*-)$_3$ or (mPEG-*a*-PCL-*a*-)$_3$, have been prepared *via* a "coupling-onto" method based on ring-opening polymerization (ROP) and Cu(I)-catalyzed azide-alkyne cycloaddition (CuAAC) "Click" chemistry. The chemical compositions and structures, as well as the molecular weights and molecular weight distributions (PDIs) of these copolymers have been fully characterized by ^{1}H NMR, FT-IR, and GPC measurements. Differential scanning calorimetry (DSC) and wide-angle X-ray diffraction (WAXD) analyses demonstrated that the thermal behaviors of the star-block copolymers strongly depended on the relative lengths of PEG and PCL blocks in the arms. The self-assembly behaviors of these amphiphilic star-block copolymers were investigated by fluorescence probe method, dynamic light scattering (DLS) and transmission electron microscopy (TEM) analyses. The results showed that they could self-assemble into spherical micelles at low concentrations and mainly formed short rod-like micelles at high concentrations. Moreover, the acid-cleavable properties of these star-block copolymers were systematically studied by ^{1}H NMR, GPC, and DLS measurements, and the results indicated that they were relatively stable in neutral pH media, but could be degraded at acidic conditions. The *in vitro* DOX release studies showed that DOX was released from drug-loaded micelles in a pH-sensitive manner. MTT assays demonstrated that these star-block copolymers possess low cytotoxicity against L929 cells and HeLa cells, and the DOX-loaded micelles exhibit higher inhibition to the proliferation of HeLa cells in comparison with free DOX. Moreover, the results from live cell imaging system and flow cytometry analysis revealed that these polymeric micelles could efficiently deliver and release DOX into the nuclei of HeLa cells. These pH-triggered shell-sheddable micelles are highly promising for the efficient intracellular delivery of hydrophobic anti-cancer drugs.

Introduction

pH-Responsive polymers can potentially be exploited in a broad range of drug delivery applications. It has been widely reported that conjugation or encapsulation of anticancer drugs into pH-sensitive polymers can significantly improve their solubility, circulation half-lives, tumor targeting and drug bioavailability.[1-5] Considering the different pH environments at the internal and external tumor tissues (for example, endocytic pathway of cells begins near the physiological pH of 7.4, while it drops to a lower pH of 5.5-6.0 in endosomes and approaches pH 4.5-5.0 in lysosomes),[2,6,7] researchers have designed some copolymers containing acid-cleavable groups, such as acetal,[8-10] hydrazone[11-13], orthoester,[14,15] and carbamate,[16] because the hydrolysis of acid-labile groups in the acidic environment of cancer cells would accelerate the dissociation of the drug-loaded micelles and further result in a rapid release of encapsulated drugs. Among them, various shaped polymers (linear-, branched-, linear-dendritic copolymers and even hydrogels) with acid-cleavable linkages have been developed.[11,15,17-20] However, the precise modulation of polymer structures is still a challenging work, and star-block copolymers containing multiple acid-labile linkages were less reported.

Compared to the linear analogues with identical molar masses, star-shaped polymers possess several features: compact structure (smaller hydrodynamic volume and radius of gyration, and therefore lower viscosity) and the multiple functionalities, which are useful in mechanical and thermal properties, rheology, solution behavior, drug loading and release properties.[21-25] As typical biomaterials approved by the United States Food and Drug Administration (FDA),[26,27] poly(ethylene glycol) (PEG) and poly(ε-caprolactone) (PCL) have been widely used to construct amphiphilic copolymers, such as diblock,[28,29] triblock,[30,31] three-arm,[32] four-arm[32,33] and multi-arm star-shaped copolymers.[34-37] In 2012, Hawker *et al*. reported a convenient one-step way to simultaneously introduce functional acetal and azide groups in the same polymer chain,[19] which provides us more opportunities to prepare pH-responsive polymers by means of highly efficient CuAAC "Click" reaction. Our group has recently utilized this

method for preparing a pH-sensitive triblock copolymer PCL-*a*-PEG-*a*-PCL, in which the acetal groups can be rapidly acid-triggered for hydrolysis.[31] These studies showed that the acid-cleavable groups introduced into PEG- and PCL-based topological copolymers would endow the polymers with excellent pH-responsive properties.

In general, star polymers comprise several polymer arms emanating from a central core. The preparation of star polymers can be mainly categorized into three strategies: "core-first", "arm-first", and "coupling-onto" methods.[24,38] The "core-first" method is growing arms from a multifunctional core that is capable of initiating polymerization of monomers in multiple sites; In the "arm-first" method, the linear polymer arms are first synthesized, followed by binding them together to form the star polymers; While the "coupling-onto" approach is highlighted by coupling of the reactive end of at least one polymer arm to a multifunctional core using some highly efficient and orthogonal reactions. Up to now, various controlled/living polymerizations including ring-opening polymerization (ROP),[39] living anionic polymerization,[40,41] atom transfer radical polymerization (ATRP),[42-45] nitroxide-mediated radical polymerization (NMP)[46] and reversible addition-fragmentation chain transfer (RAFT) polymerization[45,47,48] have been employed to generate desired multi-armed macromolecular architectures. In particular, since Sharpless proposed "Click" chemistry in 2001,[49] this technique has been become a powerful and versatile synthetic strategy because of its unique advantages, such as mild and simple reaction conditions, high efficiency and selectivity, as well as exceptional tolerance towards a wide range of functional groups and reaction conditions.[50-52] "Click" chemistry is also utilized to combine with various polymerization techniques to prepare many kinds of star polymers with controlled compositions.[23-25,53-57]

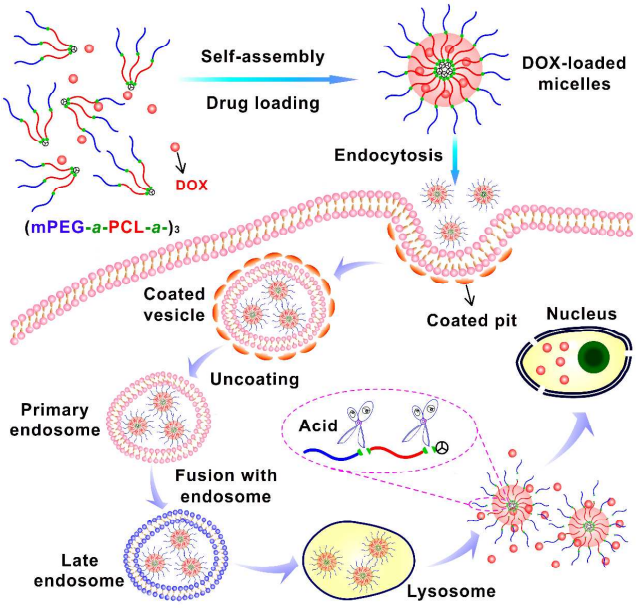

Scheme 1 Illustration of pH-sensitive shell-sheddable biocompatible micelles based on (mPEG-*a*-PCL-*a*-)$_3$ copolymer for efficient intracellular release of anti-cancer drugs triggered by acidic microenvironment inside tumor tissue.

Herein, we develop a novel strategy for the mild and precise modular synthesis of well-defined three-arm star-block copolymers comprising PEG and PCL blocks linked with six acid-cleavable acetal groups, designated as (mPEG-*a*-PCL-*a*-)$_3$. As shown in Scheme 1, the star-block copolymer can self-assemble into micelles and encapsulate the hydrophobic anti-cancer drug doxorubicin (DOX) simultaneously. The acetal linkages can be cleaved under endosomal and lysosomal acidic media once the DOX-loaded micelles were internalized by cancer cells. The shedding of hydrophilic PEG shells would result in the dissociation of micelles and subsequent fast release of DOX. To our knowledge, the synthesis of (mPEG-*a*-PCL-*a*-)$_3$ *via* a combination of ROP and CuAAC "Click" reaction have not been reported before. Therefore, this work provides a facile approach to the synthesis of novel acid-cleavable star-block copolymers with well-defined structures, which would find a great potential towards smart biomedical applications.

Experimental

Materials

Propargyl alcohol (98%, Alfa Aesar) was dried over anhydrous $MgSO_4$ for 24 h at room temperature and distilled under reduced pressure before use. Toluene (A.R., Sinopharm Chemical Reagent) and ε-CL (99%, Acros) were dried over CaH_2 for 24 h at room temperature and distilled under reduced pressure before use. Dichloromethane (CH_2Cl_2, A.R., Sinopharm Chemical Reagent) was refluxed with CaH_2 and distilled before use. Stannous octoate [Sn(Oct)$_2$, 95%, Sigma-Aldrich] was distilled under reduced pressure before use. 1, 3, 5-benzenetricarbonyl trichloride (BTT, 98%, Alfa Aesar), 4-dimethylamino pyridine (DMAP, 99%, Shanghai Medpep), poly(ethylene glycol) monomethyl ether (mPEG, $\overline{M}_n \approx 2000$ g mol^{-1}, PDI = 1.05, TCI), 2-chloroethyl vinyl ether (CEVE, 98%, TCI), pyridinium *p*-toluenesulfonate (PPTS, 98%, Acros), sodium azide (NaN_3, 98%, Sinopharm Chemical Reagent), *N*, *N*, *N*′, *N*″, *N*″-pentamethyldiethylenetriamine (PMDETA, 98%, Sigma-Aldrich), dimethyl sulfoxide (DMSO, A.R., Sinopharm Chemical Reagent), triethylamine (TEA, A.R., Sinopharm Chemical Reagent), 3-(4, 5-dimethylthiazol-2-yl)-2, 5-diphenylte-trazolium bromide (MTT, 98%, Sigma-Aldrich), DOX·HCl (99%, Beijing Zhongshuo Pharmaceutical Technology Development), and bisbenzimide Hoechst 33342 trihydrochloride (H 33342, 98%, Sigma-Aldrich) were used as received. Cuprous bromide (CuBr, 95%, Sinopharm Chemical Reagent) was purified by washing in turn with acetone, glacial acetic acid, and ethanol for three times, followed by drying under vacuum at room temperature for 24 h. THF (A.R., Sinopharm Chemical Reagent) was dried over KOH for at least two days and then refluxed over sodium wire with benzophenone as an indicator until the colour turned purple. mPEG$_{45}$-*a*-N_3 ($\overline{M}_{n,\,NMR}$ = 2150 g mol^{-1}, $\overline{M}_{n,\,GPC}$ = 3600 g mol^{-1}, PDI = 1.06) was prepared according to the procedures reported by Hawker's group.[19] Milli-Q water (18.2 MΩ cm^{-1}) was generated using a water purification system (Simplicity UV, Millipore). All the other chemicals were all analytical reagents and used as received unless otherwise mentioned.

Synthesis of tripropargyl-containing TPBTC

To a solution of propargyl alcohol (0.5 g, 8.92 mmol) and DMAP (0.9078 g, 7.43 mmol) dissolved in 50 mL of anhydrous THF stirred at 0 °C, 5-benzenetricarbonyl trichloride (BTT, 0.6577 g, 2.48 mmol) was added dropwise under a nitrogen atmosphere. The reaction was then conducted at 25 °C for 12 h. After the white precipitate formed during reaction was removed by filtration, the solvent was removed by rotary evaporation. The resulting mixture was dissolved in 60 mL of CH_2Cl_2 and washed with 10 mL of Milli-Q water, with each aqueous layer being further extracted with 30 mL of CH_2Cl_2. The organic layer was dried over anhydrous $MgSO_4$ for 1 h and evaporated to dryness by rotary evaporation. The white solid was collected and dried under vacuum at 25 °C to a constant weight (TPBTC, 0.6380 g, yield: 59.4%). ^{1}H NMR (400 MHz, $CDCl_3$, ppm): δ 2.57 (s, 3H, ***H***C≡CCH$_2$−), δ 5.00 (s, 6H, −C***H***$_2$OCO−), δ 8.94 (s, 3H, aromatic protons); ^{13}C NMR (100 MHz, $CDCl_3$, ppm): δ 53.35 (−***C***H$_2$OCO−), δ 75.89 (H***C***≡), δ 77.31 (HC≡***C***CH$_2$−), δ 130.81 and 135.45 (aromatic carbons), δ 164.15 (−O***C***O−). LC/MS *m*/*z* calcd. for $C_{18}H_{12}NaO_6$ $[M \cdot Na]^+$: 347.0532, found: 347.0515.

Synthesis of propargyl- and acetal-functionalized PCL (PA-PCL-*a*-Cl)

Propargyl-poly(ε-caprolactone) (PA-PCL) was first prepared by propargyl alcohol-initiated ROP reaction of ε-CL with $Sn(Oct)_2$ as the catalyst. Briefly, a 50 mL of dry flask was charged with $Sn(Oct)_2$ (0.405 g, 1 mmol) and 20 mL of anhydrous toluene under a nitrogen atmosphere, three exhausting-refilling nitrogen cycles were then taken to degas the solution. To this solution, ε-CL (4.5656 g, 40 mmol) and propargyl alcohol (0.1121 g, 2 mmol) were added by syringe, and the mixture was kept stirring at 90 °C for 4 h. Afterwards, the solution was concentrated and precipitated in cold diethyl ether twice. The precipitates were collected and dried under vacuum at 25 °C to a constant weight (PA-PCL$_{27}$, 4.369 g, yield: 93.4%, $\overline{M}_{n,\,NMR}$ = 3130 g mol^{-1}, $\overline{M}_{n,\,GPC}$ = 4780 g mol^{-1}, PDI = 1.10). ^{1}H NMR (400 MHz, $CDCl_3$, ppm): δ 1.33-1.45 (m, 54H, −CH$_2$C***H***$_2$CH$_2$CH$_2$O−), δ 1.59-1.72 (m, 108H, −C***H***$_2$CH$_2$C***H***$_2$CH$_2$O−), δ 2.27-2.35 (t, 54H, −COC***H***$_2$−), δ 2.48 (s, 1H, ***H***C≡CCH$_2$−), δ 3.65 (t, 2H, −C***H***$_2$OH), δ 4.04-4.10 (t, 52H, −CH$_2$C***H***$_2$O−), δ 4.68 (s, 2H, HC≡CC***H***$_2$−).

Subsequently, PA-PCL-*a*-Cl was prepared from a reaction of PA-PCL and 2-chloroethyl vinyl ether (CEVE). A typical procedure is given as follows: PA-PCL$_{27}$ (3.13 g, 1 mmol) and PPTS (0.0251 g, 0.1 mmol) were first added into a 100 mL of dry flask and purified by azeotropic drying with toluene twice. After 50 mL of anhydrous CH_2Cl_2 was added to dissolve PA-PCL$_{27}$ and PPTS, CEVE (0.5 mL, 5 mmol) was added dropwise into the solution at 0 °C under the protection of nitrogen. After stirring for 30 min at 0 °C, the reaction was quenched by adding 10 mL of 5 wt% Na_2CO_3 aqueous solution. The mixture was then diluted with 40 mL of CH_2Cl_2 and washed with 10 mL of pH buffer solution (pH 10.0), with each aqueous layer being further extracted with 20 mL of CH_2Cl_2. The organic layer was dried over anhydrous $MgSO_4$ for 1 h, and the filtrate was evaporated to dryness by rotary evaporation. The solid was redissolved in a mixture of CH_2Cl_2/THF (1/1, *v*/*v*) and precipitated in 150 mL of cold diethyl ether twice, the precipitates were collected and dried under vacuum at 25 °C to a constant weight (PA-PCL$_{27}$-*a*-Cl, 2.0743 g, yield: 64.1%, $\overline{M}_{n,\,NMR}$ = 3240 g mol^{-1}, $\overline{M}_{n,\,GPC}$ = 5360 g mol^{-1}, PDI = 1.16). ^{1}H NMR ($CDCl_3$, 400 MHz, ppm): δ 1.31-1.45 [m, 57H, −CH$_2$C***H***$_2$CH$_2$CH$_2$O−, −CH(C***H***$_3$)−], δ 1.59-1.72 (m, 108H, −C***H***$_2$CH$_2$C***H***$_2$CH$_2$O−), δ 2.27-2.35 (t, 54H, −COC***H***$_2$−), δ 2.48 (s, 1H, ***H***C≡CCH$_2$−), δ 3.44 (t, 2H, −C***H***$_2$OCH−), δ 3.63 (t, 2H, −C***H***$_2$CH$_2$Cl), δ 3.69-3.85 (br, 2H, −CH$_2$C***H***$_2$Cl), δ 4.04-4.10 (t, 52H, −CH$_2$C***H***$_2$O−), δ 4.68 (s, 2H, HC≡CC***H***$_2$−), δ 4.77 [m, 1H, −C***H***(CH$_3$)−].

Synthesis of azide- and acetal-functionalized diblock copolymer mPEG-*a*-PCL-*a*-N$_3$

To a 50 mL of dry flask, mPEG$_{45}$-*a*-N$_3$ (0.3386 g, 0.1575 mmol) and PA-PCL$_{27}$-*a*-Cl (0.486 g, 0.15 mmol) were dissolved in 20 mL of anhydrous THF, followed by three exhausting-refilling nitrogen cycles. Afterwards, CuBr (0.0215 g, 0.15 mmol) and PMDETA (0.063 ml, 0.30 mmol) were added into the mixture, and the reaction was conducted at 25 °C for 24 h. The solvent was removed under reduced pressure, diluted with 100 mL of CH_2Cl_2, and washed with 20 mL of PBS buffer solution (pH 10.0) twice, with each aqueous layer being further extracted with 20 mL of CH_2Cl_2. The combined organic layer was dried over anhydrous $MgSO_4$ for 1 h. The filtrate was concentrated and precipitated in 100 mL of cold methanol/diethyl ether (1/10, *v*/*v*) twice. The white solid was redissolved in 5 mL of THF and dialyzed (MWCO 5000) against Milli-Q water for two days. The purified diblock copolymer was obtained by lyophilization. (mPEG$_{45}$-*a*-PCL$_{27}$-*a*-Cl, 0.6169 g, yield: 76.3%, $\overline{M}_{n,\,NMR}$ = 5390 g mol^{-1}, $\overline{M}_{n,\,GPC}$ = 7080 g mol^{-1}, PDI = 1.15). ^{1}H NMR ($CDCl_3$, 400 MHz, ppm): δ 1.26 [d, 3H, −OCH$_2$CH$_2$OCH(C***H***$_3$)−], δ 1.31-1.45 [m, 57H, −CH$_2$C***H***$_2$CH$_2$CH$_2$O−, −CH(C***H***$_3$)OCH$_2$CH$_2$Cl], δ 1.59-1.72 (m, 108H, −C***H***$_2$CH$_2$C***H***$_2$CH$_2$O−), δ 2.27-2.35 (t, 54H, −COC***H***$_2$−), δ 3.38 (s, 3H, C***H***$_3$O−), δ 3.61-3.68 [t, 184H, −OC***H***$_2$C***H***$_2$O−, −OC***H***$_2$CH$_2$Cl, −CH$_2$CH$_2$C***H***$_2$OCH(CH$_3$)−], δ 3.69-3.92 (br, 4H, −OC***H***$_2$CH$_2$N−, −CH$_2$C***H***$_2$Cl), δ 4.04-4.10 (t, 52H, −CH$_2$C***H***$_2$OCO−), δ 4.55 (t, 2H, −OCH$_2$C***H***$_2$N−), δ 4.77 [m, 2H, −C***H***(CH$_3$)], δ 5.21 (s, 2H, −CC***H***$_2$O−), δ 7.74 (s, 1H, −NC***H***C−).

Subsequently, mPEG$_{45}$-*a*-PCL$_{27}$-*a*-Cl (0.539 g, 0.1 mmol) and NaN_3 (0.065 g, 1.0 mmol) were dissolved in 5 mL of DMF in a 25 mL of flask, and the reaction was stirred at 60 °C for 40 h. After removing the insoluble salt by filtration, the filtrate was concentrated under reduced pressure, diluted with 50 mL of CH_2Cl_2, and washed with 10 mL of PBS buffer solution (pH 10.0), with each aqueous layer being further extracted with 20 mL of CH_2Cl_2. The combined organic layer was dried over anhydrous $MgSO_4$ for 1 h, and the filtrate was concentrated and precipitated in 100 mL of cold diethyl ether. The precipitates were then collected and dried under vacuum at 25 °C to a constant weight (mPEG$_{45}$-*a*-PCL$_{27}$-*a*-N$_3$, 0.4393 g, yield: 81.5%, $\overline{M}_{n,\,NMR}$ = 5390 g mol^{-1}). ^{1}H NMR ($CDCl_3$, 400 MHz, ppm): δ 1.26 [d, 3H, −OCH$_2$CH$_2$OCH(C***H***$_3$)−], δ 1.31-1.45 [m, 57H, −CH$_2$C***H***$_2$CH$_2$CH$_2$O−, −CH(C***H***$_3$)OCH$_2$CH$_2$N$_3$], δ 1.59-1.72 (m, 108H, −C***H***$_2$CH$_2$C***H***$_2$CH$_2$O−), δ 2.27-2.35 (t, 54H, −COC***H***$_2$−), δ 3.38 (m, 5H, C***H***$_3$O−, −C***H***$_2$N$_3$), δ 3.61-3.68 [t, 184H, −OC***H***$_2$C***H***$_2$O−, −OC***H***$_2$CH$_2$N$_3$, −CH$_2$CH$_2$C***H***$_2$OCH(CH$_3$)−], δ 3.82 (t, 2H, −OC***H***$_2$CH$_2$N−), δ 4.04-4.10 (t, 52H, −CH$_2$C***H***$_2$OCO−), δ 4.55 (t, 2H, −OCH$_2$C***H***$_2$N−), δ 4.77 [m, 2H,

−C***H***(CH_3)], δ 5.21 (s, 2H, −CC***H***$_2$O−), δ 7.74 (s, 1H, −NC***H***C−).

Synthesis of acid-cleavable star-block copolymer (mPEG-*a*-PCL-*a*-)$_3$

The acid-cleavable star-block copolymers (mPEG-*a*-PCL-*a*-)$_3$ were synthesized *via* CuAAC reaction between mPEG-*a*-PCL-*a*-N_3 and TPBTC. Typically, in a 50 mL of dry flask, mPEG$_{45}$-*a*-PCL$_{27}$-*a*-N_3 (0.3288 g, 0.061 mmol) and TPBTC (0.0065 g, 0.02 mmol) were dissolved in 20 mL of dry THF, followed by three exhausting-refilling nitrogen cycles. Subsequently, CuBr (0.0086 g, 0.06 mmol) and PMDETA (0.025 mL, 0.12 mmol) were added into the mixture, which was further degassed by three exhausting-refilling nitrogen cycles, and the reaction was stirred at 25 °C for 24 h. The solvent was removed under reduced pressure, diluted with 50 mL of CH_2Cl_2, and washed with 5 mL of PBS buffer solution (pH 10.0) twice, with each aqueous layer being further extracted with 20 mL of CH_2Cl_2. The organic layer was dried over anhydrous $MgSO_4$ for 1 h and the filtrate was dried by rotary evaporation. The crude product was redissolved in 10 mL of CH_2Cl_2, followed by adding diethyl ether dropwise under stirring until the solution became cloudy. The solution was further stirred for 30 min, the precipitates were collected and dried under vacuum at 25 °C to a constant weight [(mPEG$_{45}$-*a*-PCL$_{27}$-*a*-)$_3$, 0.1851 g, yield: 56.1%, $\overline{M}_{n,\,NMR}$ = 16490 g mol^{-1}, $\overline{M}_{n,\,GPC}$ = 20590 g mol^{-1}, PDI = 1.07]. ^{1}H NMR ($CDCl_3$, 400 MHz, ppm): δ 1.26 [d, 9H, −OCH$_2$CH$_2$OCH(C***H***$_3$)−], δ 1.31-1.45 [m, 171H, −CH$_2$C***H***$_2$CH$_2$CH$_2$O−, −CH$_2$CH$_2$CH$_2$OCH(C***H***$_3$)−], δ 1.59-1.72 (m, 324H, −C***H***$_2$CH$_2$C***H***$_2$CH$_2$O−), δ 2.27-2.35 (t, 162H, −COC***H***$_2$−), δ 3.38 (s, 9H, C***H***$_3$O−), δ 3.61-3.68 (t, 546H, −OC***H***$_2$C***H***$_2$O−, −CH$_2$CH$_2$C***H***$_2$OCH−), δ 3.82 (t, 12H, −OC***H***$_2$CH$_2$N−), δ 4.04-4.10 (t, 156H, −CH$_2$C***H***$_2$OCO−), δ 4.55 (t, 12H, −OCH$_2$C***H***$_2$N−), δ 4.66, 4.77 [m, 6H, −C***H***(CH_3)], δ 5.21 (s, 6H, −CC***H***$_2$OCOCH$_2$−), δ 5.50 (s, 6H, −CC***H***$_2$OCOC−), δ 7.74 (s, 3H, −NC***H***CCH$_2$OCOCH$_2$−), δ 7.85 (s, 3H, −NC***H***CCH$_2$OCOC−), δ 8.82 (s, 3H, aromatic protons).

Characterizations

^{1}H NMR and ^{13}C NMR spectra were recorded on a 400 MHz NMR instrument (INOVA-400) with $CDCl_3$ as the solvent and TMS as the internal reference. The mass spectrum was performed on an Agilent 6220 Accurate-Mass TOF LC/MS instrument with acetonitrile as the solvent. Fourier transform infrared (FT-IR) spectra were performed on a Nicolet 6700 spectrometer using the KBr disk method. The number-average molecular weights and molecular weight distributions (PDIs) of polymers were recorded on a Waters 1515 gel permeation chromatography (GPC) instrument using a PLgel 5.0 μm bead size guard column (50 × 7.5 mm), followed by two linear PLgel columns (500 Å and Mixed-C), and a differential refractive index detector. THF was used as the eluent at a flow rate of 1.0 mL min^{-1} at 30 °C, and the narrowly-distributed polystyrene were used for the calibration standards. Differential scanning calorimetry (DSC) analysis was performed under nitrogen using a Q200 instrument (TA) at a heating rate of 10 °C min^{-1}. Wide-angle X-ray diffraction (WAXD) measurements were carried out on a X'Pert PRO Multiple Crystals (powder) X-ray Diffractometer using a Ni-filtered Cu Kα radiation (λ: 1.5406 Å; voltage: 40 kV; current: 40 mA) at room temperature. The samples were mounted on a circular sample holder and scanned from 5° to 35° (2θ).

Self-assembly behavior

The critical aggregation concentration (CAC) values were determined by the fluorescence probe method using pyrene as the hydrophobic probe. Typically, a predetermined pyrene solution in acetone were respectively added into a series of ampoules, acetone was then evaporated and replaced with aqueous polymer solutions at different concentrations with the range from 400 to 8 × 10^{-3} mg L^{-1}. The final concentration of pyrene in each ampoule was 6 × 10^{-6} mol L^{-1}. The samples were sonicated for 10 min, stirred at room temperature for 24 h, and analyzed on a spectrofluorometer (FLS920, Edinburgh) at the excitation wavelength of 335 nm and emission wavelength of 350 to 550 nm, with both bandwidths were set at 2 nm. From the pyrene emission spectra, the intensity ratio (I_3/I_1) of the third band (382 nm, I_3) to the first band (371 nm, I_1) was analyzed as a function of polymer concentration. The CAC value was defined as the point of intersection of two lines in the plot of fluorescence *versus* polymer concentration.

The average particle sizes ($\overline{D}_z$) and size polydispersity indices (size PDIs) of the polymeric micelles were carried out at 25 °C using a dynamic light scattering instrument (Zetasizer Nano ZS, Malvern) equipped with a 633 nm He-Ne laser and 90° collecting optics using back-scattering detection. The micelles with a concentration of 80 mg L^{-1} were prepared by directly dissolving the polymer in Milli-Q water, and stirred for three days before use. Dust particles were removed by filtering each polymer solution through a Φ 0.45 μm microfilter before measurements. The morphologies of the polymeric micelles were observed by a TEM instrument (TECNAI G^2 20, FEI) operated at an accelerating voltage of 200 kV. All the polymer solutions were prepared as described in particle sizes determination, and the sample was then prepared by a freeze-drying method.[31,58] The carbon-coated copper grid was placed on the bottom of a glass cell, which was then immediately inserted into liquid nitrogen. Subsequently, 8 μL of the micellar solution was dripped on the grid, and the solvent in its frozen solid state was directly removed without melting in a freeze-drier. The morphologies were then imaged on a normal TEM instrument at room temperature.

***In vitro* loading and release of DOX**

DOX was loaded into micelles by a dialysis method. Briefly, 10 mg of copolymer was dissolved in 2 mL of THF in a 50 mL round-bottomed flask, followed by adding 0.2 mL of DOX/DMSO stock solution (5 mg mL^{-1}). 2 mL of Milli-Q water was then added dropwise under moderate stirring, followed by dialysis (MWCO 3500) against Milli-Q water for 24 h at room temperature to remove THF and free DOX. The dialysis medium was changed for five times during the process. Finally, the DOX-loaded micelle solution was then diluted to 10 mL with Milli-Q water to a desired concentration. For determing the DOX loading content, 1 mL of the solution was lyophilized and dissolved in 4 mL of DMF. The solution was measured by fluorescence spectroscopy (FLS920, Edinburgh) with excitation at 480 nm and emission at 560 nm, and the slit width was set at 5 nm. Notably, the whole procedure was performed in the dark. The drug loading content (DLC) and drug loading efficiency (DLE) were calculated according to the following equations:

$$\text{DLC}\,(\%) = \frac{\text{Weight of DOX in micelles}}{\text{Weight of Polymers}} \times 100 \quad (1)$$

$$\text{DLE}\,(\%) = \frac{\text{Weight of DOX in micelles}}{\text{Weight of DOX in feed}} \times 100 \quad (2)$$

The DOX release from drug-loaded micelles were investigated at 37 °C in acetate buffer solution (pH 5.0, 10 mM) and phosphate buffer solution (pH 6.0 and 7.4, 10 mM). Typically, 1 mL of the as-prepared DOX-loaded micelle solution was transferred into a dialysis membrane bag (MWCO 12000-14000), which was immersed into a tube containing 20 mL of corresponding buffer solution in a shaking water bath at 37 °C. At predetermined intervals, 5 mL of the release medium was taken out and replenished with an equal volume of fresh buffer solution. Fluorescence measurement was carried out to determine the content of released DOX. All the release experiments were conducted in triplicate in the dark and the reported results were the average values with standard deviations.

In vitro cytotoxicity

A standard MTT assay was employed to evaluate the cytotoxicity of polymers against L929 cells and HeLa cells. The anti-tumor activity of DOX-loaded micelles against HeLa cells was evaluated by the MTT assay using free DOX as the control. Cells were seeded in a 96-well plate at a density of about 5×10^4 cells per well and cultured in DMEM culture medium with 10% serum and 1% penicillin/streptomycin in an incubator at 37 °C in 5% CO_2 atmosphere for 24 h. Sample with different concentrations were then added into different wells and incubated with cells for another 48 h. Afterwards, 25 μL of MTT stock solution (5 mg mL^{-1} in PBS) was added to each well. After incubation for another 4 h, DMEM medium was removed and 150 μL DMSO was added to each well. The optical density (OD) at 570 nm of each well was measured on a microplate reader (Bio-Rad 680). The absorbance values were normalized to wells in which cells were not treated with polymers. Data are presented as the average values with standard deviations.

Cellular uptake and intracellular release of DOX

The cellular uptake and intracellular release behaviors of DOX-loaded micelles were monitored against HeLa cells with a live cell imaging system (CELL'R, Olympus). Typically, HeLa cells were seeded in a Φ35 mm glass Petri dish at a density of 2×10^4 cells cm^{-2}, and the dish was located in the incubator of a live cell imaging system at 37 °C under 5% CO_2 atmosphere. The culture medium was removed after 12 h of incubation, and the cells were washed with PBS and stained with H 33342 (10 mg L^{-1}) for 15 min. Afterwards, The culture medium was then replaced with DMEM medium containing DOX-loaded micelles (0.1 mg L^{-1} of DOX). The images were then captured with an excitation wavelength of 480 nm (red) and 340 nm (blue) for 24 h. The cells treated with free DOX (0.1 mg L^{-1}) were used as the control.

Results and discussion

Synthesis and characterization of polymers

Scheme 2 shows the preparation routes with four steps: (A) synthesis of a tripropargyl-containing core molecule triprop-2-ynyl benzene-1, 3, 5-tricarboxylate (TPBTC); (B) preparation of a propargyl (PA) and acetal-functionalized PCL (PA-PCL-*a*-Cl); (C) synthesis of an azide and acetal-functionalized PEG (mPEG-*a*-N_3); (D) formation of the three-arm star-block copolymer (mPEG-*a*-PCL-*a*-)$_3$ *via* two-step CuAAC reaction. Because the TPBTC core was linked with three arms (mPEG-*a*-PCL-*a*-) by acetal groups, the star-block copolymer would be cleaved at acidic condition.

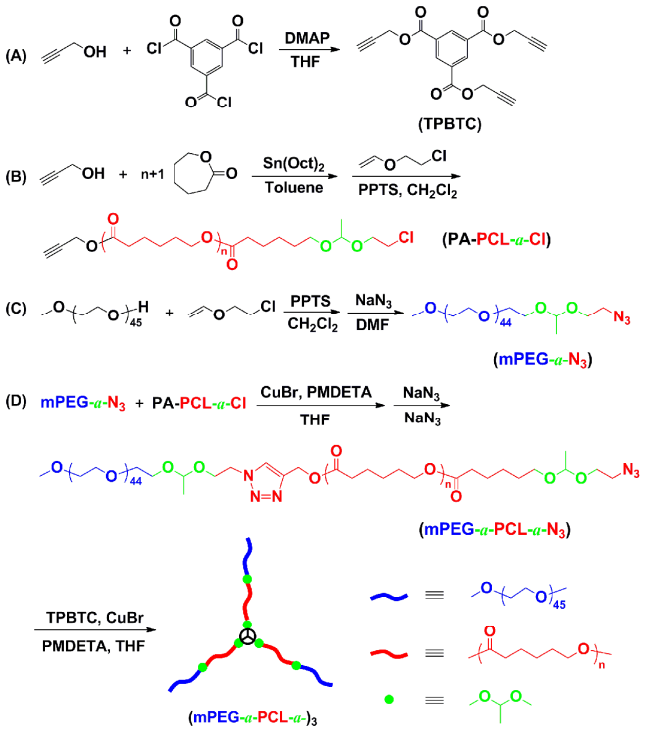

Scheme 2 Synthesis routes of acid-cleavable three-arm star-block copolymer (mPEG-*a*-PCL-*a*-)$_3$ *via* a combination of ROP and CuAAC "Click" reaction.

The chemical structure of TPBTC was confirmed by ^{1}H NMR, ^{13}C NMR and LC/MS analysis. All the characteristic signals of protons and carbon atoms in TPBTC are shown in Fig. S1(A)† and Fig. S1(B)†, respectively. In addition, the successful synthesis of TPBTC is also supported by the presence of one peak at *m/z* 347.0515 in the LC/MS spectrum, which is in good agreement with the calculated value (347.0532) for $C_{18}H_{12}NaO_6$ $[M \cdot Na]^+$. Scheme 2(B) shows the preparation procedure of propargyl- and acetal-functionalized PA-PCL-*a*-Cl. Three different monomer/initiator ratios were utilized to obtain PA-PCL with different molecular weights, and the detailed results are listed in Table 1. It can be observed that three PA-PCL samples with controlled molecular weights and relatively low PDIs (1.09-1.10) have been successfully obtained by this reaction. The ^{1}H NMR spectra of PA-PCL_{27} and PA-PCL_{27}-*a*-Cl are presented in Fig. S2(A)† and Fig. S2(B)†, respectively. All the characteristic peaks ascribed to the protons in the polymers can be found in the spectra. Moreover, compared with the spectrum of PA-PCL_{27}, the ^{1}H NMR spectrum of PA-PCL_{27}-*a*-Cl displays new chemical shifts attributed to the protons of the acetal group (peaks n and p). The molecular weights ($\overline{M}_{n,\,NMR}$) of PA-PCL and PA-PCL-*a*-Cl were calculated according to the ^{1}H NMR analysis by the following equations:

$$\overline{M}_{n,\,NMR\,(PA\text{-}PCL)} = \frac{A_j}{2A_h} \times 114.14 + 56 \quad (3)$$

$$\overline{M}_{n,\,NMR\,(PA\text{-}PCL\text{-}a\text{-}Cl)} = \overline{M}_{n,\,NMR\,(PA\text{-}PCL)} + 106 \quad (4)$$

where A_j and A_h are the integral values of the peaks j and h in Fig. S2(A)†, respectively; 114.14 is the molecular weight of one repeating unit of PCL block, 56 is the molecular weight of the propargyl group and terminal hydrogen atom, and 106 is the molecular weight of the acetal group and chlorine atom.

Table 1. Characterization data of the compositions, number-averaged molecular weights and molecular weight distributions (PDIs) of various polymers.

Samples	$\overline{M}_{n,\,theor.}$ [a] (g mol^{-1})	$\overline{M}_{n,\,NMR}$ [b] (g mol^{-1})	$\overline{M}_{n,\,GPC}$ [c] (g mol^{-1})	PDI[c]
$mPEG_{45}$	2000	2040	3180	1.05
$mPEG_{45}$-*a*-Cl	2110	2150	3570	1.07
$mPEG_{45}$-*a*-N_3	2110	2150	3600	1.06
PA-PCL_{18}	1200	2110	2930	1.10
PA-PCL_{27}	2340	3130	4780	1.10
PA-PCL_{45}	5910	5190	7030	1.09
PA-PCL_{18}-*a*-Cl	1310	2220	4060	1.18
PA-PCL_{27}-*a*-Cl	2450	3240	5360	1.16
PA-PCL_{45}-*a*-Cl	6020	5300	8810	1.19
$mPEG_{45}$-*a*-PCL_{18}-*a*-Cl	3310	4370	5840	1.11
$mPEG_{45}$-*a*-PCL_{27}-*a*-Cl	4560	5390	7080	1.15
$mPEG_{45}$-*a*-PCL_{45}-*a*-Cl	8130	7450	12860	1.19
$(mPEG_{45}$-a-PCL_{18}-*a*-$)_3$	10250	13430	12750	1.13
$(mPEG_{45}$-*a*-PCL_{27}-*a*-$)_3$	14000	16490	20590	1.07
$(mPEG_{45}$-*a*-PCL_{45}-*a*-$)_3$	24550	22510	25340	1.13

[a] Theoretical molecular weight. [b] Calculated from ^{1}H NMR spectra. [c] Determined by GPC with THF as the eluent and polystyrene as standards.

The functional precursor (mPEG-*a*-N_3) was also introduced to construct the acid-cleavable three-arm star-block copolymer. Scheme 2(C) shows the synthesis route of $mPEG_{45}$-*a*-N_3 and the chemical structure was verified by ^{1}H NMR and FT-IR analysis, as shown in Fig. S3† and Fig. S4†, respectively. The molecular weights ($\overline{M}_{n,\,NMR}$) of mPEG-*a*-N_3 was calculated according to the ^{1}H NMR analysis by the following equation:

$$\overline{M}_{n,\,NMR\,(mPEG\text{-}a\text{-}N3)} = \frac{3A_b}{4A_a} \times 44.1 + 31 + 114 \quad (5)$$

where A_a and A_b are the integral values of the peaks a and b in Fig. S3(A)†, respectively; 44.1 is the molecular weight of one repeating unit of PEG block, 31 is the molecular weight of the methoxyl group, and 114 is the molecular weight of the acetal and azide groups.

Subsequently, mPEG-*a*-N_3 was used to react with PA-PCL-*a*-Cl to yield the diblock copolymer mPEG-*a*-PCL-*a*-Cl by CuAAC reaction using CuBr/PMDETA as the catalyst system, as shown in Scheme 2(D). In order to achieve the completed reaction, the molar ratio of mPEG-*a*-N_3 to PA-PCL-*a*-Cl was set as 1.05:1. Those unreacted mPEG-*a*-N_3 could be efficiently removed by precipitating in cold methanol/diethyl ether (1/10, *v*/*v*) and dialyzing against Milli-Q water. Fig. S2(C)† shows the ^{1}H NMR spectrum of $mPEG_{45}$-*a*-PCL_{27}-*a*-Cl, from which one can find that in addition to the signals ascribed to the protons in the PCL and PEG blocks displayed in Fig. S2(B)† and Fig. S3(C)†, a new peak at δ 7.74 ppm (peak g) attributed to the characteristic proton of triazole ring can be observed. Meanwhile, the peak at δ 2.48 ppm (peak g) derived from propargyl group in PA-PCL_{27}-Cl completely disappeared in Fig. S2(C)†. FT-IR measurement was also carried out to further demonstrate the CuAAC reaction between $mPEG_{45}$-*a*-N_3 and PA-PCL_{27}-*a*-Cl. From Fig. S5†, it is clearly observed that the absorption peak at 2106 cm^{-1} attributed to the azide group completely disappeared, whereas a new strong absorption peak at 1726 cm^{-1} corresponding to the carbonyl group of PCL block appeared in Fig. S5(C)† after the CuAAC reaction. All the results discussed above demonstrated that the CuAAC reaction has been successfully achieved. The molecular weight ($\overline{M}_{n,\,NMR}$) of mPEG-*a*-PCL-*a*-Cl was calculated according to the ^{1}H NMR analysis by the following equation:

$$\overline{M}_{n,\,NMR\,(mPEG\text{-}a\text{-}PCL\text{-}a\text{-}Cl)} = \overline{M}_{n,\,NMR\,(mPEG\text{-}a\text{-}N3)} + \overline{M}_{n,\,NMR\,(PA\text{-}PCL\text{-}a\text{-}Cl)} \quad (6)$$

After that, the azide-terminated diblock copolymer mPEG-*a*-PCL-*a*-N_3 was then prepared by a nucleophilic substitution reaction between mPEG-*a*-PCL-*a*-Cl and NaN_3, and the chemical structure was confirmed by ^{1}H NMR spectrum shown in Fig. 1(A) and FT-IR spectrum shown in Fig. 2(B), respectively.

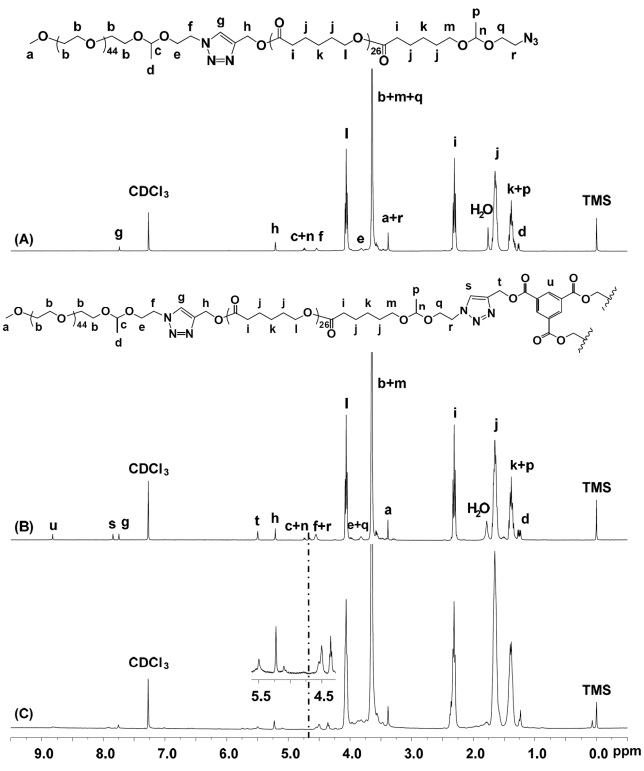

Fig. 1 ^{1}H NMR spectra of (A) $mPEG_{45}$-*a*-PCL_{27}-*a*-N_3, (B) $(mPEG_{45}$-*a*-PCL_{27}-*a*-$)_3$ and (C) the degradation products of $(mPEG_{45}$-*a*-PCL_{27}-*a*-$)_3$ in the presence of hydrochloric acid in $CDCl_3$.

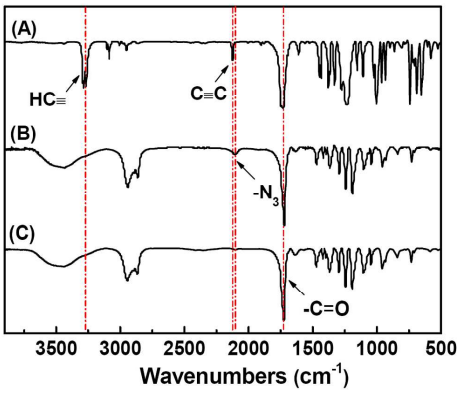

Fig. 2 FT-IR spectra of (A) TPBTC, (B) mPEG$_{45}$-*a*-PCL$_{27}$-*a*-N$_3$ and (C) (mPEG$_{45}$-*a*-PCL$_{27}$-*a*-)$_3$.

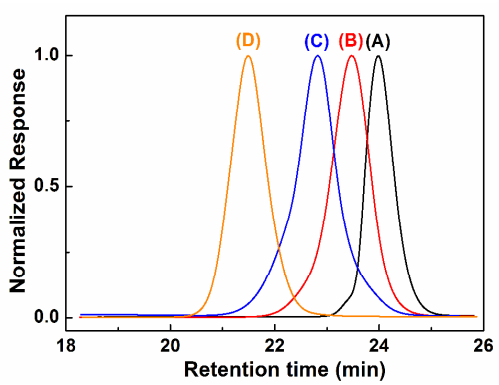

Fig. 3 GPC curves of (A) mPEG$_{45}$-*a*-N$_3$ ($\overline{M}_n$ = 3600 g mol^{-1}, PDI = 1.06), (B) PA-PCL$_{27}$-*a*-Cl ($\overline{M}_n$ = 5360 g mol^{-1}, PDI = 1.16), (C) mPEG$_{45}$-*a*-PCL$_{27}$-*a*-Cl ($\overline{M}_n$ = 7080 g mol^{-1}, PDI = 1.15), and (D) (mPEG$_{45}$-*a*-PCL$_{27}$-*a*-)$_3$ ($\overline{M}_n$ = 20590 g mol^{-1}, PDI = 1.07).

Finally, the acid-cleavable star-block copolymer (mPEG-*a*-PCL-*a*-)$_3$ was synthesized by a mild and efficient "coupling-onto" strategy based on CuAAC reaction. Considering that it was difficult to quantitatively perform the CuAAC reaction between the mPEG-*a*-PCL-*a*-N$_3$ and trifunctional TPBTC, a slightly excess of linear block copolymer was therefore used to ensure the complete formation of star copolymer and the purified product was obtained by fractional precipitation, as shown in Scheme 2(D). Fig. 3 illustrates the GPC traces of the representative homopolymers, diblock copolymer, as well as the purified star-block copolymer. One can find that all the homopolymers and diblock copolymer exhibit an unimodal distribution with relatively narrow PDI values. After CuAAC reaction, the star-block copolymer was purified by fractional precipitation for twice, and the unreacted linear polymer could be efficiently removed. As shown in Fig. 3(D), the GPC curve of (mPEG$_{45}$-*a*-PCL$_{27}$-*a*-)$_3$ displays a major distribution that shifts towards the higher molecular weight side compared with that of mPEG$_{45}$-*a*-PCL$_{27}$-*a*-Cl shown in Fig. 3(C). In Fig. 1(B), ^{1}H NMR spectrum of (mPEG$_{45}$-*a*-PCL$_{27}$-*a*-)$_3$ also displays a new characteristic signal at δ 7.85 ppm (peak s), which was ascribed to the triazole ring. There is no signal at δ 2.57 ppm ascribed to propargyl group in TPBTC [peak l, in Fig. S1(A)†], demonstrating the successful synthesis of (mPEG$_{45}$-*a*-PCL$_{27}$-*a*-)$_3$. The molecular weight ($\overline{M}_{n,\,NMR}$) of (mPEG-*a*-PCL-*a*-)$_3$ was calculated according to the ^{1}H NMR analysis by the following equation:

$$\overline{M}_{n,\,NMR\,[(mPEG\text{-}a\text{-}PCL\text{-}a\text{-})_3]} = 3 \times \overline{M}_{n,\,NMR\,(mPEG\text{-}a\text{-}PCL\text{-}a\text{-}N_3)} + M_{w\,(TPBTC)} \quad (7)$$

In addition, the FT-IR spectrum of (mPEG$_{45}$-*a*-PCL$_{27}$-*a*-)$_3$ in Fig. 2(C) shows that the absorption peaks attributed to azide and alkyne groups completely disappeared compared to Fig. 2(A) and Fig. 2(B), while the peak of the carbonyl group maintained after the "Click" reaction, which further confirmed the successful synthesis of acid-cleavable star-block copolymers. Forthermore, Table 1 summarizes the chemical compositions, number-average molecular weights and PDIs of various polymers synthesized in the present study, from which one can find that the acid-cleavabel star-block copolymers (mPEG$_{45}$-*a*-PCL$_{27}$-*a*-)$_3$ with controlled molecular weights and relatively low PDIs (<1.15) have been successfully obtained by this modular synthesis strategy.

Thermal behavior

DSC and WAXD techniques can be used to investigate the self-organization and the crystallization behavior of the copolymers in bulk and indirectly demostrate the chemical structure of polymers with different shapes.[59] In double crystalline block copolymers, the melt-crystallization behavior is rather complex. When comes to the PEG and PCL systems, since the melting temperatures of both blocks are very close to each other, coincident crystallization of both components may occur and the crystallization of one block may affect the crystallization of the other one.[60-62] The melt-crystallization behavior of star copolymers and their linear arm precursors were characterized by DSC and WAXD techniques. The DSC thermogram of mPEG$_{45}$-*a*-N$_3$ in Fig. 4(A) shows single melting peak (T_m = 49.8 °C) and crystallization peak (T_c = 29.8 °C), while the corresponding peaks of PA-PCL$_{27}$-*a*-Cl in Fig. 4(B) are located at 46.8 °C (T_m) and 29.6 °C (T_c). The WAXD pattern of mPEG$_{45}$-*a*-N$_3$ in Fig. 5(A) displays the characteristic diffraction maxima at 19.1° and 23.3°, whereas the values of PA-PCL$_{27}$-*a*-Cl in Fig. 5(B) are at 21.3° and 23.7°. As for the mPEG$_{45}$-*a*-PCL$_{27}$-*a*-Cl diblock copolymer, the DSC curve in Fig. 4(C) shows double melting peaks (T_m = 43.9 °C and 48.2 °C) and only single crystallization peak (T_c = 24.6 °C), whereas the WAXD pattern in Fig. 5(C) displays three diffraction maxima at 19.1°, 21.3° and 23.5°, indicating the coincident crystallization of PEG and PCL blocks.

In the case of (mPEG$_{45}$-*a*-PCL$_{27}$-*a*-)$_3$ star-block copolymer, the coexistence of two crystalline phases is confirmed by the presence of well-separate crystallization (T_c = 10.6 °C and 23.6 °C) and melting peaks (T_m = 38.6 °C and 44.1 °C) shown in Fig. 4(D). Meanwhile, the WAXD pattern shown in Fig. 5(D) exhibits characteristic diffraction maxima of crystalline PEG and PCL segments at 19.1°, 21.3° and 23.5°, which are in agreement with the DSC results. The topological structure made a strong influence on the thermal behavior of copolymers. In comparison with the DSC result of mPEG$_{45}$-*a*-PCL$_{27}$-*a*-Cl in Fig. 4(C), the double crystallization peaks of (mPEG$_{45}$-*a*-PCL$_{27}$-*a*-)$_3$ in Fig. 4(D) can be attributed to the localization of three PCL arms in the core, which endows strong restriction to the crystallization of PEG chains. It was also found that, if the length of PCL block was shortened from 27 units of CL to 18 ones, the crystallization of PEG chain was dominant and effectively hindered the crystallization of PCL phase. The DSC trace of (mPEG$_{45}$-*a*-PCL$_{18}$-*a*-)$_3$ star-block copolymer, which has relatively longer PEG chain, shows one melting peak at 34.5 °C (T_m) and one

crystallization peak at 8.2 °C (T_c), as shown in Fig. 4(E). Similarly, the WAXD pattern as shown in Fig. 5(E) displays the characteristic diffraction maxima of PEG at 19.1° and 23.3°, whereas those peaks related to PCL are rarely detected, which are in accordance with the DSC results.

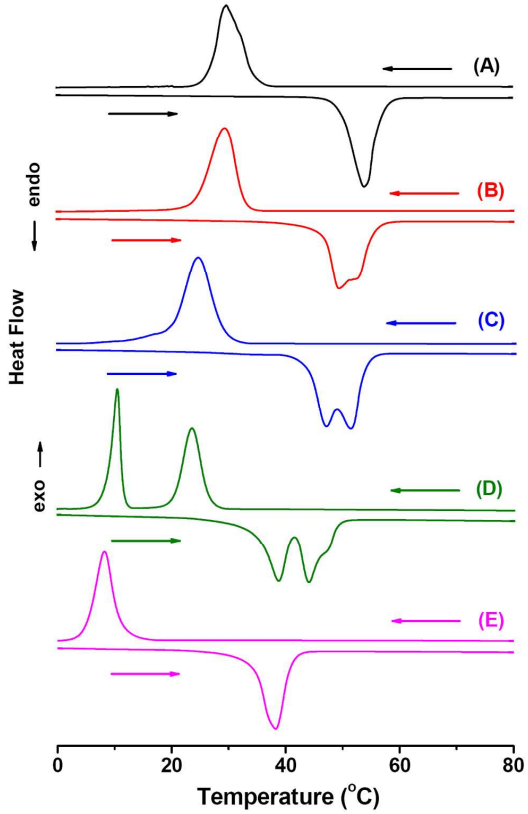

Fig. 4 DSC thermograms of (A) mPEG$_{45}$-*a*-N$_3$, (B) PA-PCL$_{27}$-*a*-Cl, (C) mPEG$_{45}$-*a*-PCL$_{27}$-*a*-Cl, (D) (mPEG$_{45}$-*a*-PCL$_{27}$-*a*-)$_3$ and (E) (mPEG$_{45}$-*a*-PCL$_{18}$-*a*-)$_3$ with a 10 °C min^{-1} scanning rate in second cooling and heating run.

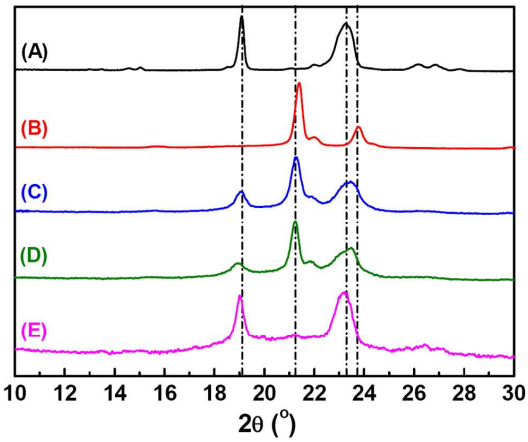

Fig. 5 WAXD patterns of (A) mPEG$_{45}$-*a*-N$_3$, (B) PA-PCL$_{27}$-*a*-Cl, (C) mPEG$_{45}$-*a*-PCL$_{27}$-*a*-Cl, (D) (mPEG$_{45}$-*a*-PCL$_{27}$-*a*-)$_3$ and (E) (mPEG$_{45}$-*a*-PCL$_{18}$-*a*-)$_3$.

Self-assembly behavior in aqueous solution

Critical aggregation concentration (CAC) is not only a strong evidence to the micellization, but also an important parameter to evaluate the stability of micelles.[63,64] The CAC values of copolymers were determined by the steady-state fluorescence probe method using pyrene as the probe, which can be an indicative of thermodynamic stability of aggregates in aqueous medium. Free-energy value is another important parameter that represents the self-assembly behavior, and it can be calculated by the equation $\Delta G° = RT \ln(X_{CAC})$, where R is the ideal gas constant, T being the Kelvin temperature and X_{CAC} represents the polymer molar fraction at CAC value.[59] The aggregate stability, assessed by low CAC data and negative $\Delta G°$ values, is mainly controlled by the chemical nature and length of hydrophobic block. Fig. 6 shows the relationship of I_3/I_1 as a function of the logarithm concentrations of copolymers, from which the CAC values were determined by intersecting the two straight lines. The CAC and $\Delta G°$ values are listed in Table 2. Both the mPEG$_{45}$-*a*-PCL$_{27}$-*a*-Cl and (mPEG$_{45}$-*a*-PCL$_{27}$-*a*-)$_3$ displayed similar CAC and $\Delta G°$ values. However, when the DP of PCL block was decreased from 27 to 18, both the CAC and $\Delta G°$ values would increase a lot. That is to say, the copolymer with longer hydrophobic segment tends to aggregate at lower concentration.

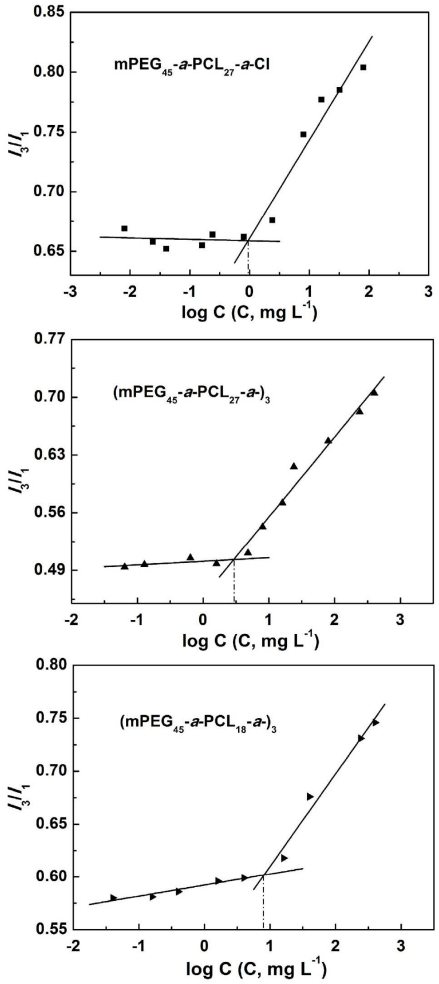

Fig. 6 Intensity ratios (I_3/I_1) as a function of the logarithm concentrations of various copolymers in pH 7.4 buffer solution.

Table 2 The CAC, X_{CAC} and $\Delta G°$ values of various copolymers in pH 7.4 buffer solution.

Samples	CAC (mg L^{-1})	X_{CAC} (mol L^{-1})	$\Delta G°$ (kJ mol^{-1})
$mPEG_{45}$-*a*-PCL_{27}-*a*-Cl	1.0	1.86×10^{-7}	-38.4
$(mPEG_{45}$-*a*-PCL_{27}-*a*-$)_3$	2.9	1.76×10^{-7}	-38.5
$(mPEG_{45}$-*a*-PCL_{18}-*a*-$)_3$	8.1	6.03×10^{-7}	-35.5

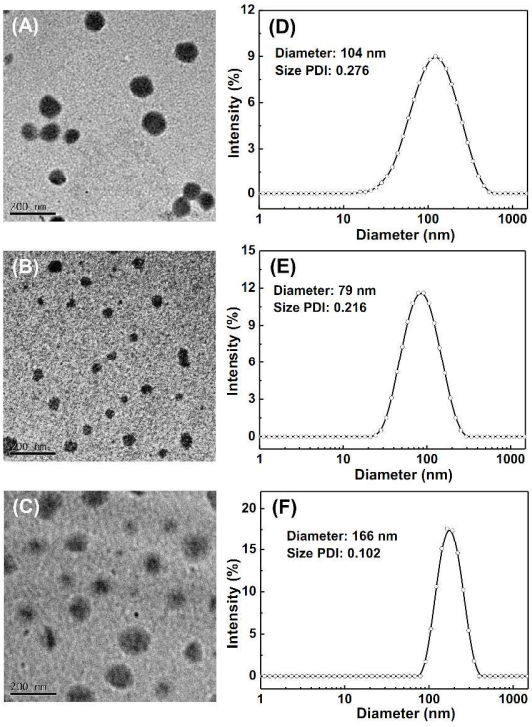

Fig. 7 TEM images of the aggregates self-assembled from different copolymers in Milli-Q water for (A) $mPEG_{45}$-*a*-PCL_{27}-*a*-Cl (80 mg L^{-1}), (B) $(mPEG_{45}$-*a*-PCL_{27}-*a*-$)_3$ (80 mg L^{-1}) and (C) DOX-loaded $(mPEG_{45}$-*a*-PCL_{27}-*a*-$)_3$ micelles (1000 mg L^{-1}), bar = 200 nm. (D), (E) and (F) are the particle size distribution curves corresponding to the samples in (A), (B) and (C), respectively.

The morphology, average particle sizes ($\bar{D}_z$) and size polydispersity indices (size PDIs) of the nanoparticles self-assembled from various copolymers were investigated by DLS and TEM measurements. Fig. 7(A, B) and Fig. S7(A)† exhibit the TEM images of the micelles obtained by the self-assembly of diblock and star-block copolymers in aqueous solution, from which we can find that these copolymers mainly form spherical micelles. The corresponding size distribution curves of the polymeric micelles measured by DLS display monomodal peaks, as shown in Fig. 7(D, E) and Fig. S7(B)†. The sizes of the aggregates formed by star-block copolymers, $(mPEG_{45}$-*a*-PCL_{27}-*a*-$)_3$ and $(mPEG_{45}$-*a*-PCL_{18}-*a*-$)_3$, were smaller than that of the linear diblock copolymer $mPEG_{45}$-*a*-PCL_{27}-*a*-Cl, indicating that the amphiphilic star polymers were prone to form more compact aggregates. The average particle sizes observed by TEM are a little smaller than those obtained from DLS. This is most likely due to the shrinkage of hydrophilic PEG shell in TEM analysis, while they can be extended into water phase in DLS measurement.

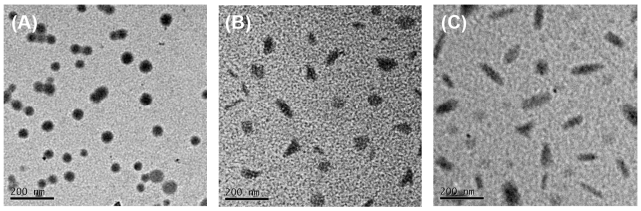

Fig. 8 TEM images of the aggregates self-assembled from $(mPEG_{45}$-*a*-PCL_{27}-*a*-$)_3$ in Milli-Q water with different concentrations: (A) 250 mg L^{-1}, (B) 500 mg L^{-1} and (C) 1000 mg L^{-1}, bar = 200 nm.

The effect of polymer concentration on the morphologies of aggregates self-assembled from star-block copolymers was also investigated. Fig. 8(A, B, C) show TEM images of the aggregates self-assembled from $(mPEG_{45}$-*a*-PCL_{27}-*a*-$)_3$ with different concentrations in Milli-Q water for 250 mg L^{-1}, 500 mg L^{-1} and 1000 mg L^{-1}, respectively. As shown in Fig. 8(A), the copolymer mainly self-assembled into spherical micelles with the diameters ranging from 30 nm to 70 nm at a low concentration of 250 mg L^{-1}. However, when the polymer concentration was increased from 250 mg L^{-1} to 500 mg L^{-1}, the morphologies of the aggregates underwent obvious changes with some short rod-like micelles appeared as shown in Fig. 8(B). With the concentration of star-block copolymer further increased to 1000 mg L^{-1}, more short rod-like micelles formed as shown in Fig. 8(C).

Acid-cleavable properties

It is well-known that pH-responsive polymers with acid-cleavable linkages are designed to keep stable at the physiological condition, but can be degraded at acidic conditions. Herein, we have investigated the acid-cleavable behavior of the star-block copolymer $(mPEG$-*a*-PCL-*a*-$)_3$ by ^1H NMR, GPC and DLS measurements. To verify the acid-responsive cleavage of the acetal linkages, 20 mg of $(mPEG_{45}$-*a*-PCL_{27}-*a*-$)_3$ was dissolved in 9 mL of THF/H_2O (2/7, *v/v*), followed by adding 1 mL of hydrochloric acid aqueous solution (36 wt%) and stirred at 25 °C for 24 h. The solution gradually became cloudy with the increase of incubation time. Finally, the reaction mixture was evaporated and freeze-dried to obtain the degradation product and its ^1H NMR spectrum is shown in Fig. 1(C), from which one can find that both the characteristic peaks attributed to PEG and PCL segments remained, but the characteristic signals derived from the protons of acetal linkages (δ 4.6-4.8 ppm) disappeared, preliminary indicating the acidic degradation of copolymers. In addition, GPC analysis was also utilized to determine the molecular weights of the degradation products. In comparison with GPC curves of $(mPEG_{45}$-*a*-PCL_{27}-*a*-$)_3$ [Fig. 9(A)], the degradation products [Fig. 9(B)] display bimodal peaks with the elution time shifting to the lower molecular weights because of the formation of corresponding PEG and PCL segments. The water-insoluble degradation part [Fig. 9(C)] exhibits almost the same elution time as that of the original PA-PCL_{27}-*a*-Cl [Fig. 2(B)], whereas the water-soluble degradation part in Fig. 9(D) exhibits a monomodal distribution and the average molecular weight agrees well with that of $mPEG_{45}$-*a*-N_3 [Fig. 2(A)]. All the aforementioned results indicates that the $(mPEG_{45}$-*a*-PCL_{27}-*a*-$)_3$ star-block copolymer can be degraded into corresponding homopolymers by the scission of acetal linkages under acidic conditions rather than the degradation of the polyester.

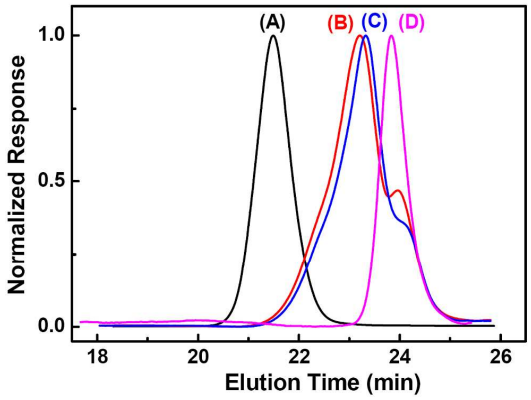

Fig. 9 GPC curves of (A) (mPEG$_{45}$-*a*-PCL$_{27}$-*a*-)$_3$, (B) degradation mixture after acidic treatment, (C) water-insoluble product after degradation and (D) water-soluble product after degradation.

On the other hand, the size change of micelles self-assembled from (mPEG$_{45}$-*a*-PCL$_{27}$-*a*-)$_3$ with the increase of hydrolysis time was monitored by DLS at pH 5.0, as shown in Fig. 10. It should be noted that no obvious size change was observed after 48 h of incubation under pH 7.4 condition. However, the size of micelles increased steadily with the increasing incubation time at pH 5.0. TEM image shows the morphology of (mPEG$_{45}$-*a*-PCL$_{27}$-*a*-)$_3$ after incubation at pH 5.0 for 48 h (Fig. S8†), and the irregular aggregates of the degraded product are clearly observed. These results could be attributed to the cleavage of acetal linkages, which resulted in the shedding of part of hydrophilic PEG shells and the increased size of micelles. The schematic illustration of this pH-dependent degradation process can be explained by Scheme 3. The stable spherical micelles were formed at pH 7.4 condition, while the cleavage of acetal linkages led to the shedding of hydrophilic PEG chains under acidic condition, resulting in the aggregation of hydrophobic PCL segments to form larger aggregates.

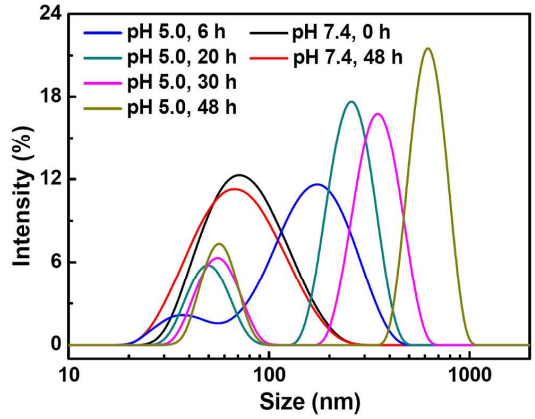

Fig. 10 The size change of (mPEG$_{45}$-*a*-PCL$_{27}$-*a*-)$_3$ micelles after incubation at pH 5.0, determined by DLS measurement. The concentrations of samples were 80 mg L^{-1}.

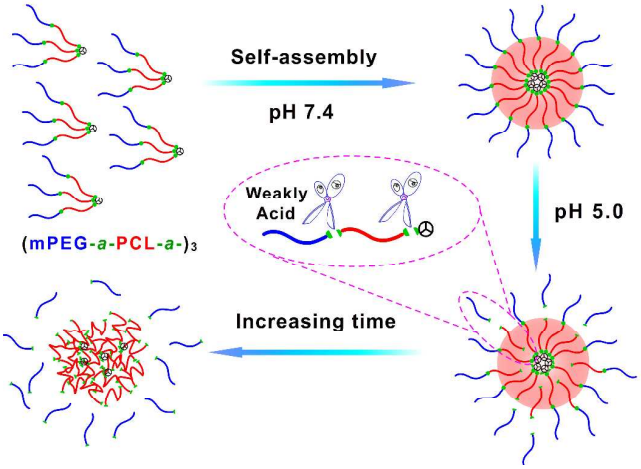

Scheme 3 Schematic illustration of the formation of micelles with acid-cleavable linkages, as well as the dissociation process of micelles in response to acidic condition.

In vitro Loading and pH-triggered release of DOX

The anti-cancer drug DOX was encapsulated into micelles by a dialysis method. Fig. 7(C) exhibits the TEM image of the DOX-loaded (mPEG$_{45}$-*a*-PCL$_{27}$-*a*-)$_3$ micelles, from which we can find that these copolymers mainly formed spherical micelles. Table 3 shows the particle sizes ($\bar{D}_z$), size polydispersities (size PDIs), drug loading content (DLC) and drug loading efficiency (DLE) of various DOX-loaded micelles. The results showed that the sizes of all three DOX-loaded micelles were smaller than 200 nm. In this study, the theoretical DLC values were set to 10 wt%. The DOX-loaded (mPEG$_{45}$-*a*-PCL$_{27}$-*a*-)$_3$ micelles had higher DLC and DLE values than that of linear diblock copolymer mPEG$_{45}$-*a*-PCL$_{27}$-*a*-Cl. What's more, when the DP of PCL block was decreased from 27 to 18, the DLC and DLE values simultaneously decreased. This is because longer hydrophobic segments attribute to larger hydrophobic core and provides more space for oil-soluble drug, which exhibits an enhancement of drug encapsulating ability.

Table 3 Properties of micelles self-assembled from various copolymers.

Samples	Size [a] (nm)	Size PDI [a]	DLC [b] (wt%)	DLE [b] (wt%)
mPEG$_{45}$-*a*-PCL$_{27}$-*a*-Cl	136 ± 2	0.199	2.05	20.5
(mPEG$_{45}$-*a*-PCL$_{27}$-*a*-)$_3$	165 ± 2	0.144	3.04	30.4
(mPEG$_{45}$-*a*-PCL$_{18}$-*a*-)$_3$	103 ± 2	0.276	2.03	20.3

[a] Determined by DLS measurement. [b] Determined by fluorescence measurement.

To investigate the effect of pH values on drug release, the *in vitro* release experiments of DOX were performed in three different buffer solutions of pH 5.0, 6.0 and 7.4, respectively. Fig. 11 shows the cumulative release curves of DOX for various copolymers at different pH values. Remarkably, the results showed that DOX was released from DOX-loaded micelles much faster at acidic condition than that at physiological condition. Furthermore, approximately 80% of DOX was released at pH 5.0 from DOX-loaded micelles in 32 h, whereas 60% was released at

pH 6.0 at the same condition. In contrast, about 40% of DOX release was observed after 32 h at pH 7.4 under the same condition. The pH-sensitive release behavior of polymeric micelles can be ascribed to the scission of the acetal linkages at the junction between PEG and PCL segments, leading to the dissociation of the star-block copolymer micelles.

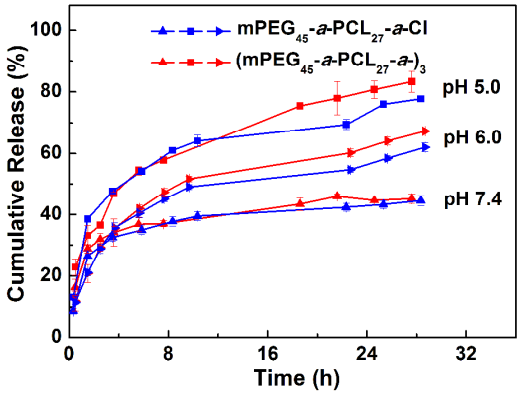

Fig. 11 *In vitro* release of DOX from various DOX-loaded polymeric micelles at 37 °C at different pH conditions.

In vitro cytotoxicity and anti-tumor assay

Biocompatibility is one of the most important properties to be considered in selecting biomedical materials. Fig. 12 shows the *in vitro* cytotoxicity of $mPEG_{45}$-*a*-PCL_{27}-*a*-Cl, ($mPEG_{45}$-*a*-PCL_{27}-*a*-)$_3$ and ($mPEG_{45}$-*a*-PCL_{18}-*a*-)$_3$ against L929 cells and HeLa cells, which were evaluated by MTT assay. The viabilities of L929 cells incubated with different samples are all above 80% after 48 h incubation, demonstrating the favorable biocompatibility of these copolymers.

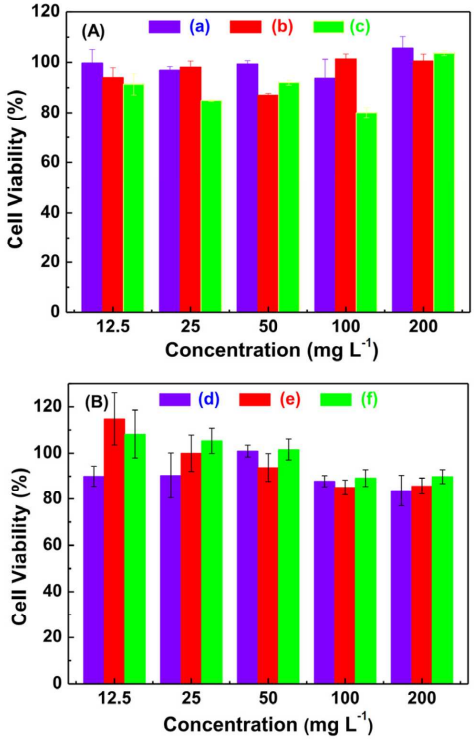

Fig. 12 Cell viability of (A) L929 cells and (B) HeLa cells incubated with (a, d) $mPEG_{45}$-*a*-PCL_{27}-*a*-Cl, (b, e) ($mPEG_{45}$-*a*-PCL_{27}-*a*-)$_3$ and (c, f) ($mPEG_{45}$-*a*-PCL_{18}-*a*-)$_3$ at different concentrations for 48 h.

The *in vitro* anti-tumor activity of DOX-loaded micelles against HeLa cells was tested by MTT assay using using free DOX as the control. The results in Fig. 13 show that the viabilities of HeLa cells incubated with DOX-loaded micelles and free DOX were decreased with increasing DOX concentrations. The DOX dosage required for inhibitory concentration to produce 50% cell death (IC_{50}) were about 0.43 and 1.20 mg L^{-1}, respectively, indicating that the DOX-loaded micelles exhibited higher inhibition to the proliferation of HeLa cells after 48 h culture in comparison with free DOX. The higher anti-tumor activity of DOX-loaded micelles over free DOX implied that DOX was efficiently delivered and released into HeLa cells.

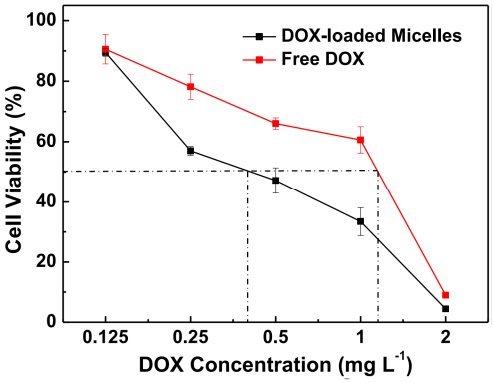

Fig. 13 Anti-tumor activity of DOX-loaded ($mPEG_{45}$-*a*-PCL_{27}-*a*-)$_3$ micelles and free DOX against HeLa cells as a function of DOX concentrations for 48 h incubation.

Intracellular release of DOX

The cellular uptake and intracellular drug release behaviors of DOX-loaded micelles were monitored using a live cell imaging system, which could synchronously record the dynamic uptake process and the variation of fluorescence intensity inside HeLa cells. The cell nuclei were stained with H 33342 (blue). As shown in Fig. 14(A), DOX fluorescence was observed in HeLa cells after incubated with DOX-loaded ($mPEG_{45}$-*a*-PCL_{27}-*a*-)$_3$ micelles for 4 h, indicating efficient internalization of DOX-loaded micelles and release of DOX inside cells. After cultured with DOX-loaded micelles for 12 h, DOX fluorescence was observed in the nuclei of HeLa cells, and the longer incubation time (20 h) resulted in stronger DOX fluorescence in the nuclei of HeLa cells. In contrast, minimal DOX fluorescence was observed in HeLa cells after cultured with free DOX for 20 h, as shown in Fig. 14(B). Flow cytometry analysis was further investigated to study the endocytosis process. Fig. S9† evidently reveals that the relative geometrical mean fluorescence intensities (GMFI) of the internalized DOX-loaded micelles and free DOX by HeLa cells increased with the incubation time. The results showed a slight higher cellular uptake of DOX-loaded micelles than free DOX after 20 h incubation. These results confirm that DOX-loaded micelles are likely more efficiently retained inside HeLa cells and have enhanced cytotoxicity as compared to free DOX. Similar results have been also reported previously.[65-68] These studies showed that the cellular distribution of DOX-loaded polymeric micelles and free DOX are different. They demonstrated that DOX-loaded micelles are internalized into cells *via* an endocytosis mechanism, while free DOX entered into the cells by a passive diffusion process. Therefore, free DOX can enter into

cells fast at first, but is then pumped out of the cells quickly. As for the micellar DOX, although it enters into the cells at a lower rate than free DOX, it may not be pumped out of cells during a relatively long periord.

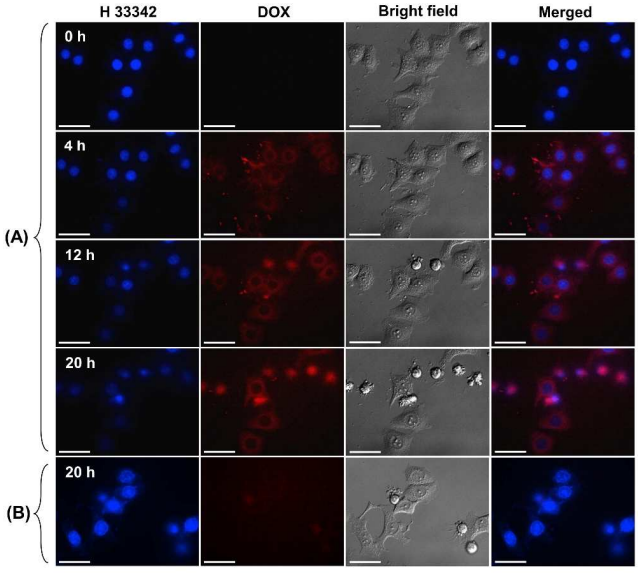

Fig. 14 Live cell imaging system images of HeLa cells incubated with (A) DOX-loaded ($mPEG_{45}$-*a*-PCL_{27}-*a*-)$_3$ micelles and (B) free DOX for different times. The DOX dosage was 0.1 mg L^{-1}. For each panel, images from left to right show cell nuclei stained by H 33342 (blue), DOX fluorescence in cells (red), bright field of cells, and overlays of the blue and red images. The scale bars are 50 μm in all images.

Conclusions

A facile methodology based on a combination of ROP and CuAAC "Click" chemistry was utilized to synthesize novel amphiphilic star-block copolymers with six acid-cleavable linkages. Two polymer precursors were first synthesized, including an acetal- and azide-functionalized PEG (mPEG-*a*-N_3), as well as an acetal- and propargyl-containing PCL (PA-PCL-*a*-Cl). Conjugation of these preformed polymer building blocks has been achieved *via* CuAAC reaction to form a diblock copolymer with two acetal linkages (mPEG-*a*-PCL-*a*-Cl). After transferring the chlorine group to azide group, the subsequent CuAAC reaction between mPEG-*a*-PCL-*a*-N_3 and a tri-functional core molecule triprop-2-ynyl benzene-1, 3, 5-tricarboxylate (TPBTC) to yield the well-defined three-arm star-block copolymer (mPEG-*a*-PCL-*a*-)$_3$. ^{1}H NMR, FT-IR and GPC measurements demonstrated that the resultant three-armed copolymers possessed controlled molecular weights and relatively low PDI values (<1.15). These amphiphilic star-block copolymers could self-assemble into spherical micelles at low concentrations and short rod-like micelles at high concentrations in aqueous solution. These micelles were relatively stable at physiological condition but degraded at acidic medium. In addition, the cytotoxicity tests showed that these star block copolymers possessed good biocompatibility. The DOX-loaded micelles exhibited a pH-dependent release manner, and they could efficiently release DOX into tumor cells and significantly enhance drug efficacy.

Acknowledgements

The authors gratefully acknowledge financial supports from the National Natural Science Foundation of China (21374066, 21304061 and 21074078), Natural Science Foundation of Jiangsu Province for Rolling Support Project (BK2011045), China Postdoctoral Science Foundation (2013M531396), Natural Science Foundation of Jiangsu Higher Education Institutions (13KJB150034), a Project Funded by the Priority Academic Program Development (PAPD) of Jiangsu Higher Education Institutions, Suzhou Science and Technology Program for Industrial Application Foundation (SYG201429), and Soochow-Waterloo University Joint Project for Nanotechnology from Suzhou Industrial Park. Mr. Jian Hu would like to thank the financial support from the Innovative Graduate Research Program of Jiangsu Province (KYLX_1222).

Notes and references

College of Chemistry, Chemical Engineering and Materials Science, Suzhou Key Laboratory of Macromolecular Design and Precision Synthesis, Jiangsu Key Laboratory of Advanced Functional Polymer Design and Application, Soochow University, Suzhou 215123, P. R. China. Tel:+86 512 65882047; E-mail: phni@suda.edu.cn (P. H. Ni); jlhe@suda.edu.cn (J. L. He)

† Electronic Supplementary Information (ESI) available. See DOI: 10.1039/b000000x/

1 G. S. Kwon and T. Okano, *Adv. Drug Deliver. Rev.*, 1996, **21**, 107-116.
2 C. Deng, Y. J. Jiang, R. Cheng, F. H. Meng and Z. Y. Zhong, *Nano Today*, 2012, **7**, 467-480.
3 K. Kataoka, A. Harada and Y. Nagasaki, *Adv. Drug Deliver. Rev.*, 2012, **64**, 37-48.
4 A. Rösler, G. W. M. Vandermeulen and H. A. Klok, *Adv. Drug Deliver. Rev.*, 2012, **64**, 270-279.
5 Z. S. Ge and S. Y. Liu, *Chem. Soc. Rev.*, 2013, **42**, 7289-7325.
6 S. Ganta, H. Devalapally, A. Shahiwala and M. Amiji, *J. Control. Release*, 2008, **126**, 187-204.
7 E. S. Lee, Z. G. Gao and Y. H. Bae, *J. Control. Release*, 2008, **132**, 164-170.
8 E. R. Gillies, A. P. Goodwin and J. M. J. Fréchet, *Bioconjugate Chem.*, 2004, **15**, 1254-1263.
9 R. Jain, S. M. Standley and J. M. J. Fréchet, *Macromolecules*, 2007, **40**, 452-457.
10 C. Tonhauser, C. Schüll, C. Dingels and H. Frey, *ACS Macro Lett.*, 2012, **1**, 1094-1097.
11 Y. Bae, S. Fukushima, A. Harada and K. Kataoka, *Angew. Chem., Int. Ed.*, 2003, **42**, 4640-4643.
12 L. J. Zhu, C. L. Tu, B. S. Zhu, Y. Su, Y. Pang, D. Y. Yan, J. L. Wu and X. Y. Zhu, *Polym. Chem.*, 2011, **2**, 1761-1768.
13 J. Z. Du, X. J. Du, C. Q. Mao and J. Wang, *J. Am. Chem. Soc.*, 2011, **133**, 17560-17563.
14 J. Cheng, R. Ji, S. J. Gao, F. S. Du and Z. C. Li, *Biomacromolecules*, 2012, **13**, 173-179.
15 J. Heller, J. Barr, S. Y. Ng, K. S. Abdellauoi and R. Gurny, *Adv. Drug Deliver. Rev.*, 2002, **54**, 1015-1039.
16 T. Liu, X. J. Li, Y. F. Qian, X. L. Hu and S. Y. Liu, *Biomaterials*, 2012, **33**, 2521-2531.
17 R. Tomlinson, M. Klee, S. Garrett, J. Heller, R. Duncan and S. Brocchini, *Macromolecules*, 2002, **35**, 473-480.
18 Y. Jin, L. Song, Y. Su, L. J. Zhu, Y. Pang, F. Qiu, G. S. Tong, D. Y. Yan, B. S. Zhu and X. Y. Zhu, *Biomacromolecules*, 2011, **12**, 3460-3468.
19 K. Satoh, J. E. Poelma, L. M. Campos, B. Stahl and C. J. Hawker, *Polym. Chem.*, 2012, **3**, 1890-1898.
20 H. Wei, R. X. Zhuo and X. Z. Zhang, *Prog. Polym. Sci.*, 2013, **38**, 503-535.

21 T. Higashihara, M. Nagura, K. Inoue, N. Haraguchi and A. Hirao, *Macromolecules*, 2005, **38**, 4577-4587.
22 Y. L. Zhao, T. Higashihara, K. Sugiyama and A. Hirao, *Macromolecules*, 2007, **40**, 228-238.
23 G. Lapienis, *Prog. Polym. Sci.*, 2009, **34**, 852-892.
24 O. Altintas, A. P. Vogt, C. Barner-Kowollik and U. Tunca, *Polym. Chem.*, 2012, **3**, 34-45.
25 K. Kempe, A. Krieg, C. R. Becer and U. S. Schubert, *Chem. Soc. Rev.*, 2012, **41**, 176-191.
26 L. S. Nair and C. T. Laurencin, *Prog. Polym. Sci.*, 2007, **32**, 762-798.
27 S. N. S. Alconcel, A. S. Baas and H. D. Maynard, *Polym. Chem.*, 2011, **2**, 1442-1448.
28 E. K. Park, S. B. Lee and Y. M. Lee, *Biomaterials*, 2005, **26**, 1053-1061.
29 H. L. Sun, B. N. Guo, R. Cheng, F. H. Meng, H. Y. Liu and Z. Y. Zhong, *Biomaterials*, 2009, **30**, 6358-6366.
30 Y. Zhang and R. X. Zhuo, *Biomaterials*, 2005, **26**, 6736-6742.
31 H. R. Wang, J. L. He, M. Z. Zhang, Y. F. Tao, F. Li, K. C. Tam and P. H. Ni, *J. Mater. Chem. B*, 2013, **1**, 6596-6607.
32 K. H. Kim, G. H. Cui, H. J. Lim, J. Huh, C. H. Ahn and W. H. Jo, *Macromol. Chem. Phys.*, 2004, **205**, 1684-1692.
33 C. L. Peng, M. J. Shieh, M. H. Tsai, C. C. Chang and P. S. Lai, *Biomaterials*, 2008, **29**, 3599-3608.
34 F. Wang, T. K. Bronich, A. V. Kabanov, R. D. Rauh and J. Roovers, *Bioconjugate Chem.*, 2005, **16**, 397-405.
35 P. F. Gou, W. P. Zhu and Z. Q. Shen, *Biomacromolecules*, 2010, **11**, 934-943.
36 L. Sun, W. Liu and C. M. Dong, *Chem. Commun.*, 2011, **47**, 11282-11284.
37 C. Gao, Y. Wang, P. F. Gou, X. Cai, X. D. Li, W. P. Zhu and Z. Q. Shen, *J. Polym. Sci., Part A: Polym. Chem.*, 2013, **51**, 2824-2833.
38 H. F. Gao and K. Matyjaszewski, *Prog. Polym. Sci.*, 2009, **34**, 317-350.
39 D. J. A. Cameron and M. P. Shaver, *Chem. Soc. Rev.*, 2011, **40**, 1761-1776.
40 T. Higashihara, M. Hayashi and A. Hirao, *Prog. Polym. Sci.*, 2011, **36**, 323-375.
41 W. B. Zhang, J. L. He, K. Yue, C. Liu, P. H. Ni, R. P. Quirk and S. Z. D. Cheng, *Macromolecules*, 2012, **45**, 8571-8579.
42 K. Matyjaszewski and J. H. Xia, *Chem. Rev.*, 2001, **101**, 2921-2990.
43 J. Z. Du and Y. M. Chen, *Macromolecules*, 2004, **37**, 3588-3594.
44 H. F. Gao and K. Matyjaszewski, *Macromolecules*, 2006, **39**, 4960-4965.
45 W. A. Braunecker and K. Matyjaszewski, *Prog. Polym. Sci.*, 2007, **32**, 93-146.
46 C. J. Hawker, A. W. Bosman and E. Harth, *Chem. Rev.*, 2001, **101**, 3661-3688.
47 E. Setijadi, L. Tao, J. Q. Liu, Z. F. Jia, C. Boyer and T. P. Davis, *Biomacromolecules*, 2009, **10**, 2699-2707.
48 R. T. A. Mayadunne, J. Jeffery, G. Moad and E. Rizzardo, *Macromolecules*, 2003, **36**, 1505-1513.
49 H. C. Kolb, M. G. Finn and K. B. Sharpless, *Angew. Chem., Int. Ed.*, 2001, **40**, 2004-2021.
50 D. Fournier, R. Hoogenboom and U. S. Schubert, *Chem. Soc. Rev.*, 2007, **36**, 1369-1380.
51 M. Meldal and C. W. Tornøe, *Chem. Rev.*, 2008, **108**, 2952-3015.
52 P. L. Golas and K. Matyjaszewski, *Chem. Soc. Rev.*, 2010, **39**, 1338-1354.
53 H. F. Gao, K. Min and K. Matyjaszewski, *Macromol. Chem. Phys.*, 2007, **208**, 1370-1378.
54 C. A. Bell, Z. F. Jia, J. Kulis and M. J. Monteiro, *Macromolecules*, 2011, **44**, 4814-4827.
55 C. N. Ye, G. D. Zhao, M. J. Zhang, J. Z. Du and Y. L. Zhao, *Macromolecules*, 2012, **45**, 7429-7439.
56 C. Boyer, A. Derveaux, P. B. Zetterlund and M. R. Whittaker, *Polym. Chem.*, 2012, **3**, 117-123.
57 C. J. Dürr, L. Hlalele, A. Kaiser, S. Brandau and C. Barner-Kowollik, *Macromolecules*, 2013, **46**, 49-62.
58 H. Zhao, Q. J. Chen, L. Z. Hong, L. Zhao, J. F. Wang and C. Wu, *Macromol. Chem. Phys.*, 2011, **212**, 663-672.
59 G. Maglio, F. Nicodemi, C. Conte, R. Palumbo, P. Tirino, E. Panza, A. Ianaro, F. Ungaro and F. Quaglia, *Biomacromolecules*, 2011, **12**, 4221-4229.
60 B. Bogdanov, A. Vidts, A. Van Den Bulcke, R. Verbeeck and E. Schacht, *Polymer*, 1998, **39**, 1631-1636.
61 J. H. An, H. S. Kim, D. J. Chung and D. S. Lee, *J. Mater. Sci.*, 2001, **36**, 715-722.
62 R. V. Castillo and A. J. Müller, *Prog. Polym. Sci.*, 2009, **34**, 516-560.
63 Y. B. Zhang, C. Wu, Q. Fang and Y. X. Zhang, *Macromolecules*, 1996, **29**, 2494-2497.
64 W. L. Zhang, J. L. He, Z. Liu, P. H. Ni and X. L. Zhu, *J. Polym. Sci. Part A: Polym. Chem.*, 2010, **48**, 1079-1091.
65 L. B. Luo, J. Tam, D. Maysinger and A. Eisenberg, *Bioconjugate Chem.*, 2002, **13**, 1259-1265.
66 R. Savic, L. Luo, A. Eisenberg and D. Maysinger, *Science*, 2003, **300**, 615-618.
67 Y. Y. Diao, H. Y. Li, Y. H. Fu, M. Han, Y. L. Hu, H. L. Jiang, Y. Tsutsumi, Q. C. Wei, D. W. Chen and J. Q. Gao, *Int. J. Nanomed.*, 2011, **6**, 1955-1962.
68 H. Y. Shao, M. Z. Zhang, J. L. He and P. H. Ni, *Polymer*, 2012, **53**, 2854-2863.

Polymer Chemistry

Graphical Abstract

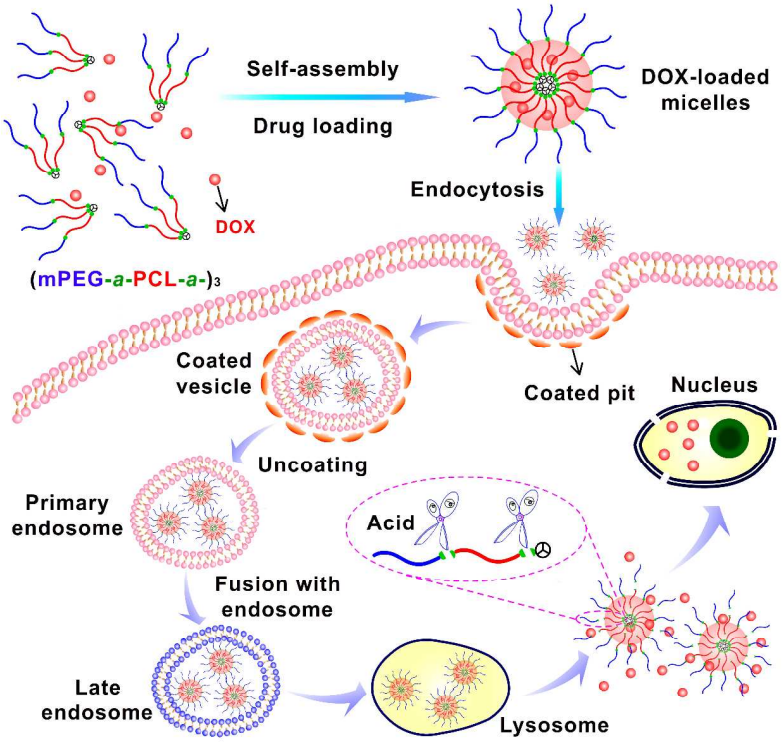

A series of well-defined three-arm star-block copolymers (mPEG-*a*-PCL-*a*-)$_3$ linked with acid-cleavable acetal groups have been prepared and used for pH-triggered delivery of doxorubicin.